15 Design and Applications of Oscillating Optical Tweezers for Direct Measurements of Colloidal Forces

H. DANIEL OU-YANG
Department of Physics, Lehigh University, Bethlehem, Pennsylvania 18015

15.1. INTRODUCTION

Optical tweezers, first developed by A. Ashkin et al. almost three decades ago,[1] have found wide use both in biological applications[2] and in colloid–polymer applications.[3–6] The technique became truly user friendly when Ashkin and co-workers demonstrated that it is possible to use a single beam with large gradient force to form an optical trap (also known as optical tweezers) for colloidal particles.[7] A review of optical tweezers applications that covers the development and many applications published between 1970 and 1995 can be found in an article by Kuo.[8]

In this chapter we demonstrate an approach that utilizes the phase-sensitive detection of the dynamic position of a single colloidal particle undergoing a forced oscillation driven by optical tweezers. By measuring the particle's position, we can calculate the dynamic forces on the particle.[9] This approach differs from that of conventional applications of optical tweezers where the optical trap is usually stationary. The advantage of using oscillating optical tweezers is that one can use it to measure frequency-dependent, dynamic properties of polymer–colloid systems at the colloidal level. The phase-sensitive lock-in method measures the phase shift and displacement of the oscillating particle relative to the oscillating optical tweezers. It can be shown that phase-sensitive measurements provide a greater sensitivity for dynamical measurements than most other techniques. Phase-sensitive measurements

Colloid–Polymer Interactions: From Fundamentals to Practice, Edited by Raymond S. Farinato and Paul L. Dubin
ISBN 0-471-24316-7

also have an advantage over direct displacement measurements in that they are less prone to the optical contrast variation that usually occurs in optical microscopy.

In what follows, we start with a brief description of the principle of optical tweezers trapping individual colloidal particles. Although there are several approaches to deal with the theory of optical trapping of particles, we choose the electrostatic approximation. It is probably the easiest to understand, and it is sufficient for someone who wishes to design a similar system.

We then review the equation of motion of a particle in a forced harmonic motion. For simplicity, we treat the medium as viscoelastic with constant viscosity and elasticity. Because we can explore high frequencies, the Stokes drag is modified to include frequency-dependent viscous drag and inertia terms; the latter includes not only the particle mass but also a part related to the frequency-dependent momentum transfer to the surrounding liquid. The equation of motion is solved to give the time-dependent displacement and phase shift of the particle's motion in the laboratory reference frame. When the displacement and phase shift are measured relative to the center of the optical trap, we can use expressions derived for the (moving) optical tweezers reference frame.

Following the theoretical treatment, an experimental setup with the necessary optical components is given. Three modes of detection are described, including direct imaging, the single-beam forward-scattering method, and the dual-beam forward-scattering method. The direct-imaging method is a laboratory frame measurement. It is easy to set up but fails at high frequencies. The forward-scattering method measures a particle's motion in the reference frame of the oscillating laser. It has an excellent high-frequency response but is insensitive at very low frequency. A dual-beam method, with one laser beam oscillating and the other stationary, measures a particle's motion in the laboratory frame and provides good response at both low and intermediate frequencies.

All three methods of detection are tested against the theoretical treatment. We ran these tests on individual colloidal particles in water, in water–glycerol mixtures, and in low-concentration polymer solutions. Most of the results are obtained using polystyrene latex spheres. Some results are from measurements of surfactant-stabilized oil droplets in water. The experimental results agree well with our theoretically calculated predictions.

The theory presented here for solutions with constant viscosity and elasticity can be extended readily to frequency-dependent viscoelastic polymer–colloid systems. One possible application is to study the microviscoelasticity of colloidal particles embedded in polymer gels.[10] Another potential application of this technique is to study the interactions between a pair of particles, each held by an optical tweezers.

15.2. PRINCIPLE OF OPTICAL TWEEZERS

By strongly focusing a laser beam, a very strong electric field is formed at the focal point, and a large electric field gradient is formed in both the axial (the laser propagation direction) and radial directions. A sufficiently steep field gradient can

create a force on a colloidal particle large enough to counter Brownian motion, thus yielding a stable optical trap in all three dimensions. The balance of gradient and scattering forces in the axial direction causes the potential minimum for the trapped particle to be slightly downstream from the focal point of the lens. The achievement of axial stability, due to the availability of high numerical aperture (NA) objective lenses, makes the trap suitable for a wider range of applications. The magnitudes of the forces are generally quoted to be about 1 picoNewton per milliwatt (pN/mW) of power at the trap site. Because of their relatively noninvasive nature, laser tweezers are ideal for probing individual colloids and cells in their microscopic environments.

Several theoretical approaches have been proposed to explain the physics of laser trapping of dielectric particles. The simplest is an electrostatic model, such as the parallel-plate capacitor model: The potential energy of the system (capacitor plus dielectric) is lowered when a dielectric material is drawn into the capacitor. Optical tweezers can be explained in the same manner: Particles of higher (at optical frequencies) dielectric constant than the surroundings are drawn into the high electric field provided by the tightly focused laser beam. The fact that the laser electric field oscillates at high frequency does not matter because, as shown below, the potential energy of the particle in the field is proportional to the square of the field strength so that the particle can follow the direct current (DC) component potential whereas the second harmonic frequency is much too high for particles to follow.

However, the electrostatic model is not complete. The problem is that the electric field produced by a laser is not electrostatic—rather it is a traveling electromagnetic (EM) wave. A traveling EM field exerts radiation pressure on the surfaces on which it impinges. In other words, the laser beam tends to push the particle in the direction of laser propagation. Trapping stability depends on the competition between the scattering force in the direction of beam propagation, proportional to intensity, and the gradient force, proportional to the gradient of intensity. It is known that not only will lower dielectric constant particles be ejected from the trap, but so will hollow particles and highly reflective materials.[11] For a more precise description, the Mie or Rayleigh scattering models must be used for particles comparable to, or smaller than, the size of the optical trap. When a particle is much larger than the size of the trap, a geometrical optics model should be used to calculate the trapping force.[12]

The potential energy of a homogeneous, linear dielectric particle in an electric field E is given by[13]

$$U = \frac{1}{2}\int \mathbf{D} \cdot \mathbf{E}^* \, d^3x \tag{15.1}$$

where $\mathbf{D}$ is the electric displacement vector equal to $\varepsilon\mathbf{E}$, where ε is the dielectric constant at optical frequencies. The difference in potential energy is

$$\Delta U = U_2 - U_1 = \frac{1}{2}\int [\mathbf{D}_2 \cdot \mathbf{E}_2^* - \mathbf{D}_1 \cdot \mathbf{E}_1^*] d^3x$$

$$= \frac{1}{2}\int [\mathbf{D}_1 \cdot \mathbf{E}_2^* - \mathbf{D}_2 \cdot \mathbf{E}_1^*]\, d^3x + \frac{1}{2}\int (\mathbf{E}_1 + \mathbf{E}_2^*) \cdot (\mathbf{D}_2 - \mathbf{D}_1^*)\, d^3x \quad (15.2)$$

where U_2 (U_1) is the energy when the particle is inside (outside) the trap. If the source charge density is assumed unchanged, the second integral on the right-hand side of Eq. (15.2) vanishes, in which case, Eq. (15.2) is reduced to[13]

$$\Delta U = \frac{1}{2}\int [\varepsilon_1 \mathbf{E}_1 \cdot \mathbf{E}_2^* - \varepsilon_2 \mathbf{E}_2 \cdot \mathbf{E}_1^*] d^3x \quad (15.3)$$

Assuming harmonic fields, we have

$$\mathbf{E} = \mathbf{E}_c\, e^{-i\omega t}$$

$$\mathbf{D} \cdot \mathbf{E}^* = \varepsilon |\mathbf{E}|^2 = \varepsilon |\mathbf{E}_c|^2 \quad (15.4)$$

Because we require $|\mathbf{E}|^2$ to be real, the amplitude $\mathbf{E}_c$ must be either purely real or purely imaginary. Thus

$$\mathbf{E}_1 \cdot \mathbf{E}_2^* = \mathbf{E}_1^* \cdot \mathbf{E}_2$$

$$\Delta U = \frac{1}{2}\int (\varepsilon_1 - \varepsilon_2) \mathbf{E}_1^* \cdot \mathbf{E}_2\, d^3x \quad (15.5)$$

It can be shown that for a dielectric sphere in an external field,[13]

$$\mathbf{E}_2 = \left(\frac{3\varepsilon_1}{\varepsilon_2 + 2\varepsilon_1}\right)\mathbf{E}_1 \quad (15.6)$$

And thus,

$$\Delta U = \frac{3\varepsilon_1}{2}\left(\frac{3\varepsilon_2 - \varepsilon_1}{\varepsilon_2 + 2\varepsilon_1}\right)\int_{V_2} |\mathbf{E}_1|^2\, d^3x \quad (15.7)$$

where V_2 is the volume of the particle. Assuming that the radius of the particle is the same size as or smaller than the trap spot size, and that the electric field is approximately uniform over the particle volume, we can rewrite Eq. (15.7):

$$\Delta U = -\frac{3n_1^2\varepsilon_0}{2}\left(\frac{n_2^2 - n_1^2}{n_2^2 + 2n_1^2}\right)|\mathbf{E}_1|^2\, V_2 \quad (15.8)$$

where n is the index of refraction, ε_0 is the dielectric permitivity of free space. Here, we have used $\varepsilon = K\varepsilon_0$, and $K \approx n^2$. Thus, when $n_2 > n_1$, $U_2 < U_1$ and the energy is lower if the particle is in the trap. For example, at optical frequencies, the index of refraction for water is $n_{water} = 1.33$, and for polystyrene spheres, $n_{ps} = 1.57$; micron-sized polystyrene spheres in water can be trapped easily.

Since we will need only to calculate the trapping forces in the radial direction, we will not discuss the rather complicated calculation of the axial trapping force. All we need for the present application is a large enough NA objective so that the particle is stable axially. In what follows, we present an electrostatic argument for the radial component of the gradient force.

In order to estimate the radial trapping force, we rewrite the potential energy in terms of the intensity via the time averaged Poynting vector:

$$I = <\mathbf{S}> = \frac{1}{2}\frac{1}{\mu_1 n_1 c}|\mathbf{E}_1|^2 = \frac{c\varepsilon_0 n_1}{2}|\mathbf{E}_1|^2$$

$$I = I_0 e^{-r^2/R^2} \tag{15.9}$$

where c is the speed of light in vacuum, μ is the magnetic permeability, and r is the radial position measured from the center of the trap. A Gaussian intensity profile with a $1/e$ width of R at the center of the trap has been assumed for the radial direction, and the potential energy measured relative to a particle at infinity is

$$U = \frac{-3V_2 n_1}{c}\left(\frac{n_2^2 - n_1^2}{n_2^2 + 2n_1^2}\right) I_0 e^{-r^2/R^2} \tag{15.10}$$

Now the force F can be found for a particle with a radial displacement from the center of the trap:

$$\mathbf{F} = -\nabla U = -\frac{6rV_2 n_1}{cR^2} I_0 \left(\frac{n_2^2 - n_1^2}{n_2^2 + 2n_1^2}\right) e^{-r^2/R^2}\hat{r}$$

$$\equiv -k_{ot} r e^{-r^2/R^2}\hat{r} \tag{15.11}$$

For small displacements the force is a Hooke's law force with spring constant k_{ot} that is, $F = k_{ot} r$. For a polystyrene sphere ($n_2 = 1.57$, radius $a = 0.5$ μm) in water ($n_1 = 1.33$) and assumed power at the trap ($R = 0.5$ μm) of 1 mW the spring constant is approximately 8 mdyn/cm. At a displacement of $r \sim 0.25R$ the force is approximately 1 pN. A comparison of the linear approximation with the force given by Eq. (15.11) is shown in Figure 15.1. It is calculated that the linear approximation is good to within 4% when the particle is displaced about $0.2\,R$ from the center of the trap or within 10% when particle is displaced about $0.32\,R$.

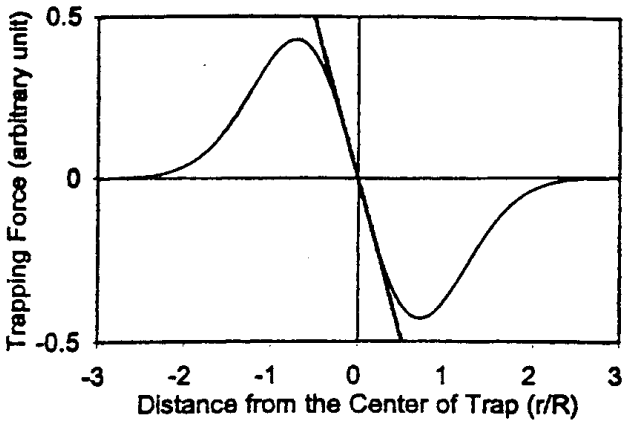

FIGURE 15.1 Comparison of the Hooke's law force (linear approximation) with the force given by Eq. (15.11).

15.3. EQUATION OF MOTION FOR A COLLOIDAL PARTICLE IN FORCED OSCILLATION IN A VISCOELASTIC MEDIUM

An individual particle in suspension can be forced into an oscillatory motion by optical tweezers that are steered by a piezoelectric transducer (PZT) controlled mirror. A single particle of radius a, set in motion (say, along the x axis with velocity v) experiences the following forces: (1) a springlike force $-k_{ot}x$, exerted by the optical tweezers; (2) the viscous force $-6\pi\eta av$, due to the Stokes drag in solution; and (3) an elastic restoring force $-kx$, where k is the effective spring constant of the solution of viscosity η. In a viscoelastic medium, both the viscosity and elasticity depend on frequency; for simplicity, we assume both are constant. However, because we consider oscillations over a broad oscillation frequency range, we need to include the frequency-dependent hydrodynamic modification terms to the Stokes drag.[14] Figure 15.2 illustrates all the forces experienced by a particle in a viscoelastic medium.

The equation of motion for the particle is

$$m^*\ddot{x} + 6\pi\eta^* a\dot{x} + (k_{ot} + k)x = k_{ot}A\cos(\omega t) \tag{15.12}$$

where m^* is the effective mass of the particle, a is the radius of the colloidal particle, η^* is the effective viscosity, k is the elastic modulus of the solution, and A is the amplitude of the tweezers' oscillation of frequency ω. It is important to note that the effective mass m^* includes not only the bare mass of the particle m_0 but also the inertia of the liquid around the particle when the particle is set into an oscillating motion. According to Landau and Lifshitz,[14] the effective mass m^* can be expressed as

$$m^* = m_0 + \frac{2\pi}{3}a^3\rho_s + 3\pi a^2\sqrt{\frac{2\eta_s\rho_s}{\omega}} \tag{15.13}$$

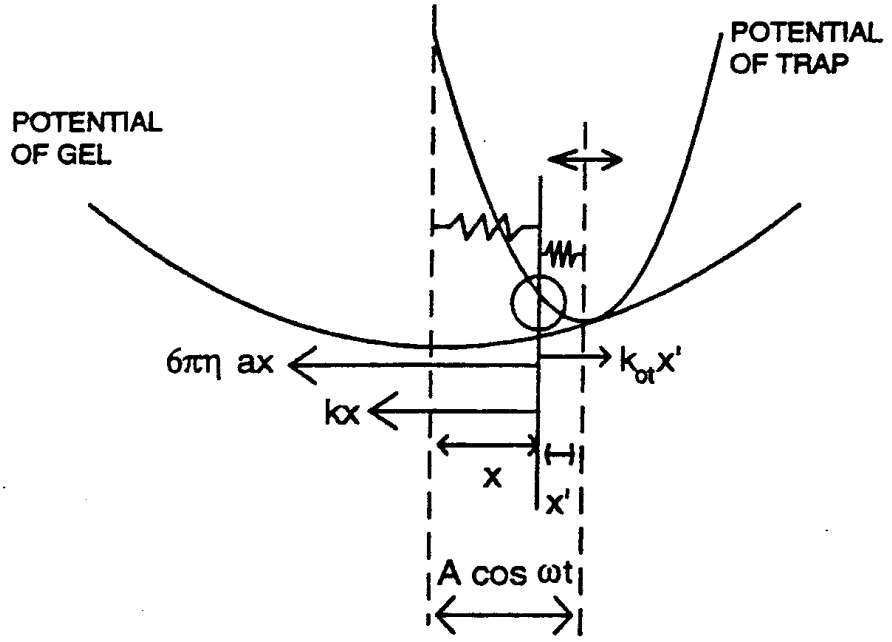

FIGURE 15.2 Forces on a single particle set in forced oscillation in a viscoelastic medium.

and the effective viscosity η^* can be expressed as

$$\eta^* = \eta_s\left(1 + \sqrt{\frac{a^2\rho_2\omega}{2\eta_2}}\right) \tag{15.14}$$

where ρ_s and η_s are the solution density and viscosity, respectively. Equation (15.12) has a steady-state solution:

$$x(t) = D(\omega)\cos(\omega t - \delta(\omega)) \tag{15.15}$$

where the amplitude and the phase shift of the response are

$$D(\omega) = \frac{k_{ot}A}{\sqrt{(k_{ot} + k - m^*\omega^2)^2 + m^{*2}\beta^2\omega^2}} \qquad \delta(\omega) = \tan^{-1}\frac{m^*\beta\omega}{k_{ot} + k - m^*\omega^2} \tag{15.16}$$

where

$$\beta = \frac{6\pi\eta^* a}{m^*} \tag{15.17}$$

In Figure 15.3*a*, we show the calculated phase shift versus log(ω) for a 1.0-μm-diameter polystyrene particle in water (density = 1 g/cm^3, η_s = 0.01 poise). The spring

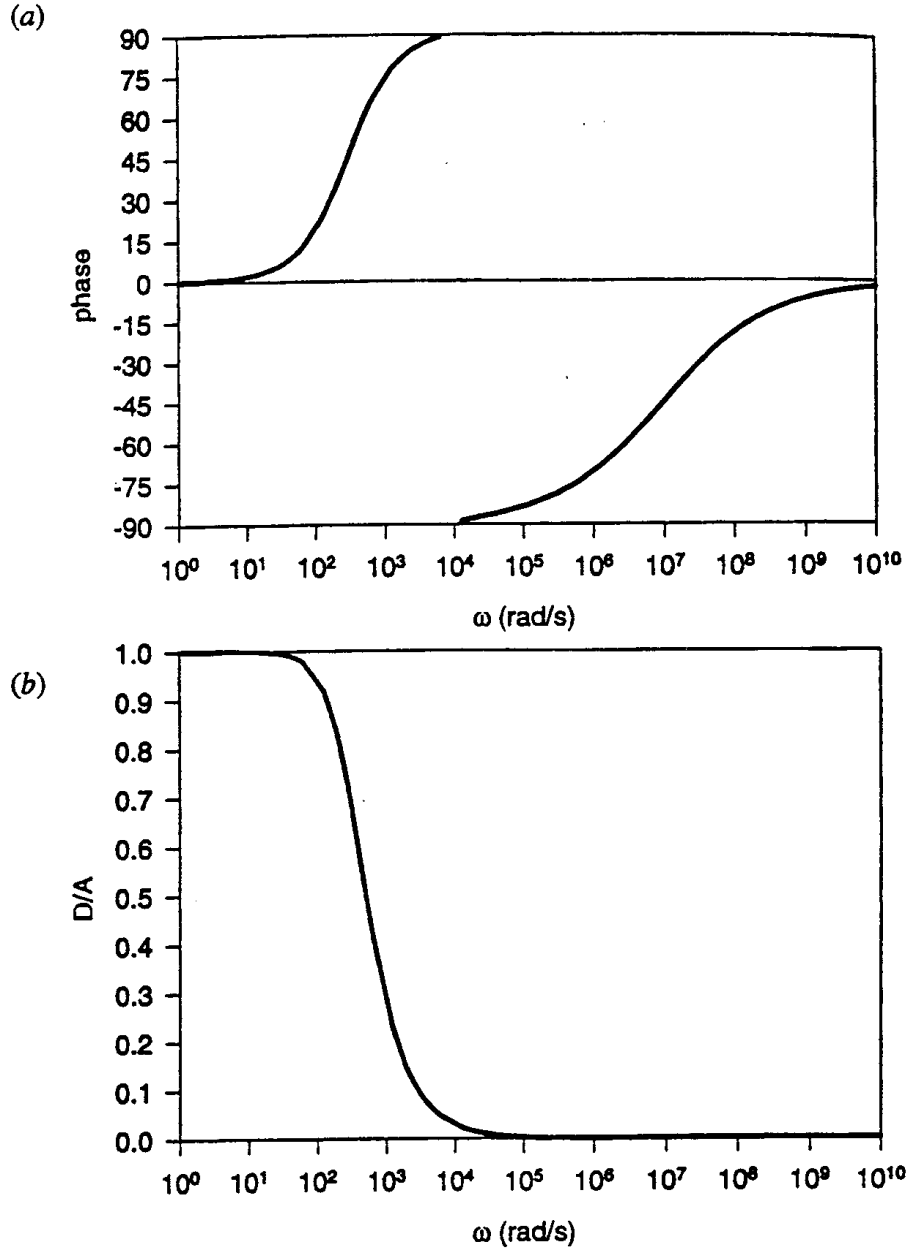

FIGURE 15.3 (*a*) Phase shift vs. log(ω) for a 1.0-μm diameter polystyrene particle in water (density = 1 g/cm^3, η_s = 0.01 poise). The spring constant k_{ot} is 3 mdyn/cm. (*b*) Relative displacement *D*/*A* vs. log(ω) for a 1.0-μm polystyrene particle (density 1.05 g/cm^3) in water (density = 1 g/cm^3, η_s = 0.01 poise). The spring constant k_{ot} is 3 mdyn/cm.

constant k_{ot} is 3 mdyn/cm. In Figure 15.3*b*, we show the calculated *D*/*A* versus log(ω) in the same system. We can see that for most systems of interest the system is highly overdamped, and both $D(\omega)$ and $\delta(\omega)$ vary appreciably over the range $0 < \omega < 10^4$ rad/s. This allows for measurement of the viscoelastic properties of the polymer solution in the frequency range of $0 < \omega < 10^4$ rad/s (shear rate range up to 10^3 to 10^5 s^{-1}). It is therefore feasible to determine the spring constant of the trap from the phase

[$\delta(\omega)$] and displacement [$D(\omega)$] measurements made on polystyrene particles in water, as water is not elastic in our frequency range (<7 kHz) and the viscosity of water is a known function of temperature.

In the next section, we describe the experimental setup and the procedures to calibrate the spring constant k_α of the optical tweezers.

15.4. EXPERIMENTAL SETUP

Here we introduce a setup that allows us to measure the motion of a colloidal particle undergoing forced oscillation, and we describe the phase lock-in detection technique. A schematic of the experimental setup for both single-beam and dual-beam optical tweezers is shown in Figure 15.4. In this diagram, we include all three methods of

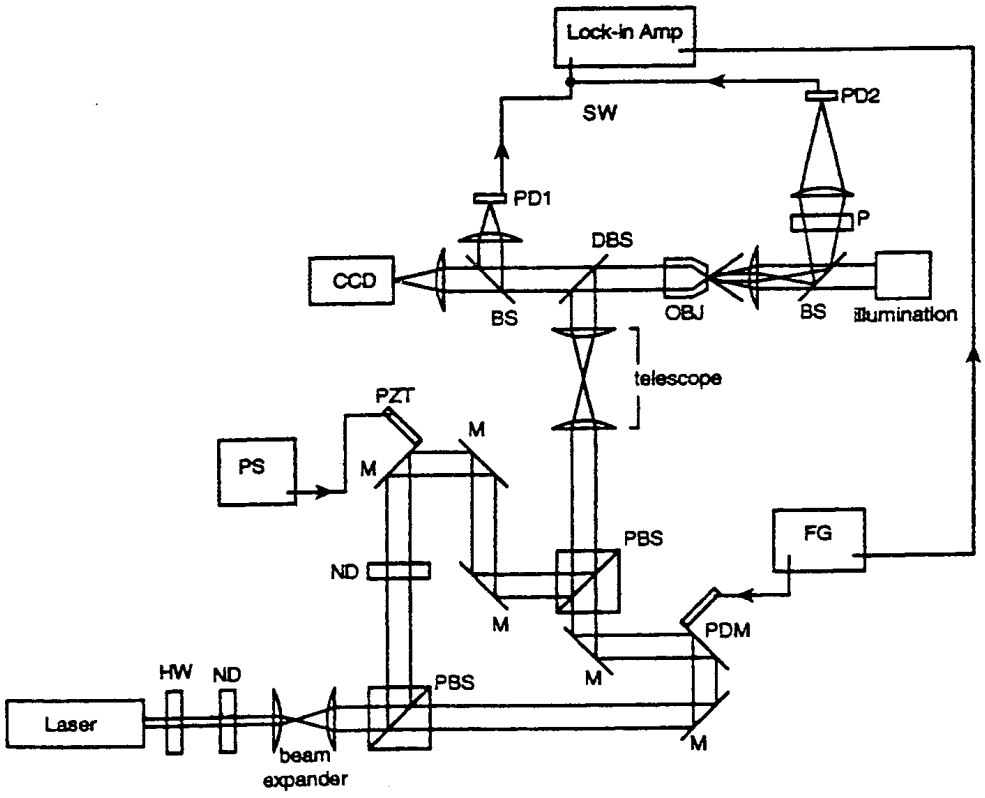

FIGURE 15.4 Schematic of the experimental setup of optical tweezers. HW is a half wave plate, ND a neutral density filter, PBS a polarizing beam splitter, M a mirror, PS a power supply for piezoelectric-driver (PZT), PDM a piezoelectric-driven mirror, FG function generater, BS a beam splitter, DBS a dichroic beam splitter, which reflects the green laser light and allows the illuminating light to pass. The OBJ is the high NA objective lens, PD1 and PD2 are splitted photodiode detectors, P a polarizer and SW a switch to allow signal from PD1 or PD2 to go to the lock-in amplifier. The sample chamber and the trapped particle, both not shown, are located directly to the right of OBJ.

detection: direct imaging, single-beam forward scattering, and dual-beam forward scattering.

As shown in Figure 15.4, our optical tweezers are built on an Olympus IX-70 inverted microscope with an Olympus Plan-Apo 100X (N.A. 0.5–1.35) oil-immersion objective lens. The laser is a Spectra-Physics Millennia Nd:YVO_4 laser at a wavelength of 532 nm (frequency-doubled, maximum power 5.5 W). The laser beam is steered by a PZT-driven mirror (Physik Instrumente, P830-40). A sinusoidal signal created by a Stanford Research Systems frequency synthesizer (SRS DS-345) is fed in a piezoelectric driver (Physik Instrumente, P863) to drive the steering mirror. A CCD (MTI CCD72) camera is used to generate a video image of the trapped particle for viewing and optical alignment. The actual measurements of the particle motions are made on the signal detected by a split photodiode detector (Hamamatsu S4204). The output electrical current signal from the split photo diode detector is fed into a lock-in amplifier (SRS 830). The reference signal is taken from the frequency synthesizer (SRS DS-345) that is used to drive the mirror. The lock-in amplifier measures the magnitude and the phase shift of the signal from the photodiode detector relative to that of the driving signals. A beam split from the beam reflected off the steering mirror can also be detected by a separate photodiode detector for determination of the frequency dependence of the steering mirror's displacement and phase shift. Note that the phase shift described in Eq. (15.16) is the relative phase shift of the particle motion to the mirror motion. The displacement described in Eq. (15.16) is the relative motion of the measured particle's displacement to the laboratory reference frame. The amplitude A of the motion of the optical tweezers is, to a good approximation, linearly proportional to the amplitude of the motion of the mirror.

15.5. EXPERIMENTAL RESULTS AND DISCUSSIONS

15.5.1. Direct Imaging Method

By imaging the trapped particle onto a split photodiode detector (PD1 in Fig. 15.4), we are actually creating a shadow of the particle in a bright background. When the particle is set into motion by the oscillating tweezers, the light distribution, with a dark spot near the center of the split photodiode detector, changes spatially with time. The lock-in amplifier analyzes the photo currents measured by the split photodiode PD1 and provides a measure of the magnitude and phase of the particle's motion. The lock-in amplification technique suppresses random noises caused by the particle's Brownian motion and other sources of noise caused by fluctuation of the bright background.

We tested the direct imaging method by measuring the phase shift of a 1.1-μm-diameter polystyrene latex sphere in water, from which we obtained the measured optical tweezers' spring constant k_{ot}. Using the same spring constant, we are able to determine the viscosity of dilute polymer solutions in water and to compare our data with direct viscosity measurements. The polymer used was 100,000 g/mol polyethyleneoxide (PEO) with both ends capped with a 16-carbon alkyl group

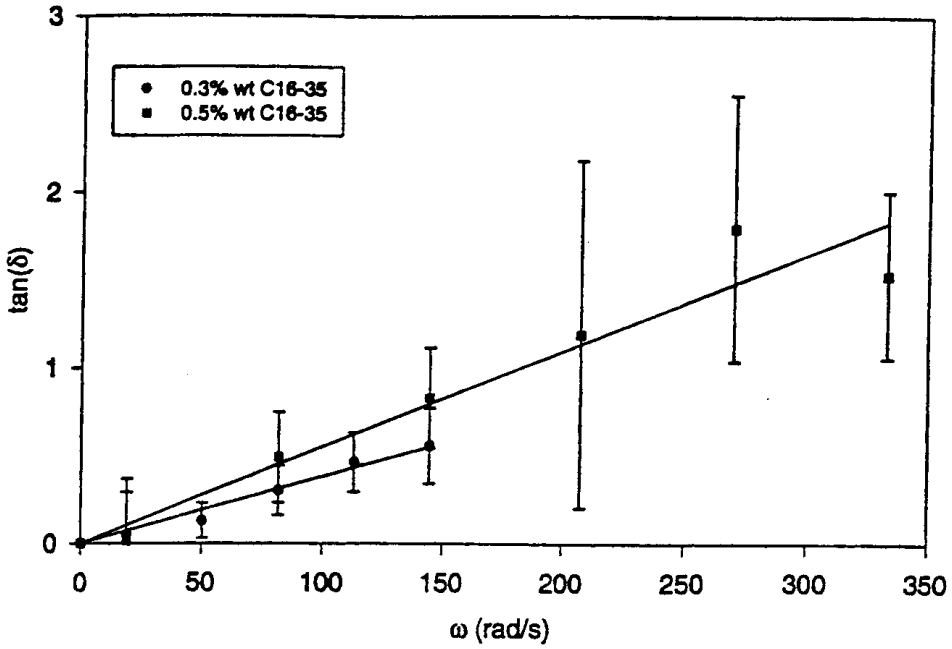

FIGURE 15.5 Plot of tan δ vs. angular frequency ω for C16-100 PEO in water solution.

(C16-100 PEO). Figure 15.5 shows a plot of tan δ versus angular frequency ω. The linear dependence in the plot is expected from Eq. (15.16). With a known spring constant, we can determine the solution viscosities of the polymer solutions. Figure 15.6 shows a comparison of the data obtained by this method and that obtained with

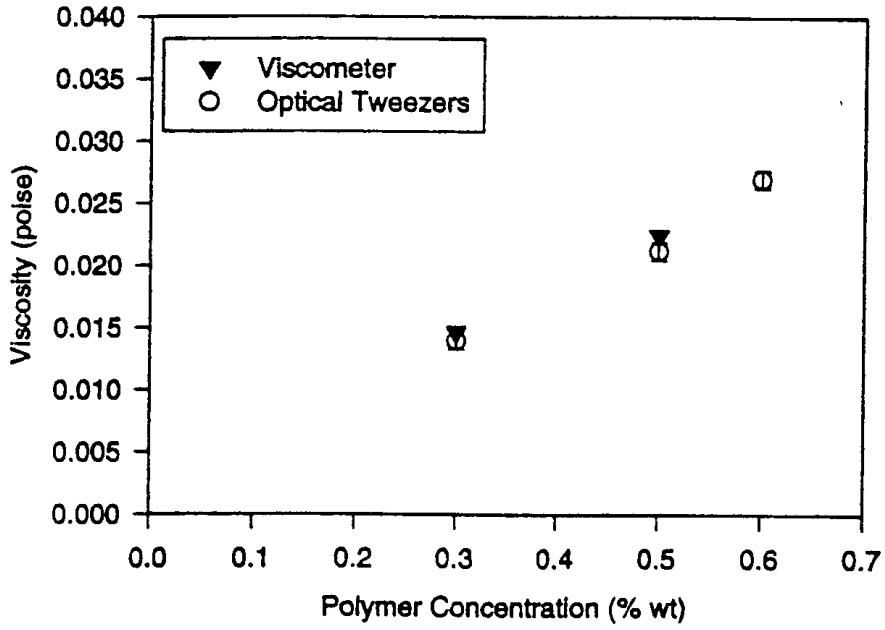

FIGURE 15.6 Comparison of viscosities measured by the optical tweezers and by a capillary viscometer.

a capillary viscometer; both methods are at shear rates less than 100 s^{-1}. The direct imaging method works well for low frequencies, but the bright background noise sets an intrinsic limit on the range of frequency response. High-frequency response can be accomplished by forward-scattering methods, as shown below.

15.5.2. Forward-Scattering Method

The motion of the trapped particle relative to the optical tweezers affects the forward-scattering pattern created by the laser. We can use the time variation of the forward-scattering intensity distribution at a split photodiode (PD2 in Fig. 15.4) to measure the desired particle motion in the trap.[15] The concept of the detection is given in Figure 15.7, where a split photodiode is positioned at the back focal plane (BFP′) of the condenser. As shown in Figure 15.7, the trapped particle can be treated as a lens that collimates the laser beam and projects the forward scattering into a tight spot on the split photodiode. When the particle is at the center of the optical trap, as shown in (15.7*a*), the forward-scattering light is projected to the center of the split photodiode, yielding a zero photo current. When the particle is away from the center of the trap, as shown in (15.7*b*), the forward-scattered light is projected off-center of the photodiode, yielding a photo current proportional to the displacement of the particle from the center of the trap.When the trapped particle undergoes oscillation in the direction perpendicular to the laser beam, the forward-scattering spot executes a similar motion at the position of the split photodiode. It should be noted, however, that the signal so obtained is a measure of the motion of the particle relative to the trapping beam center—a moving reference frame.

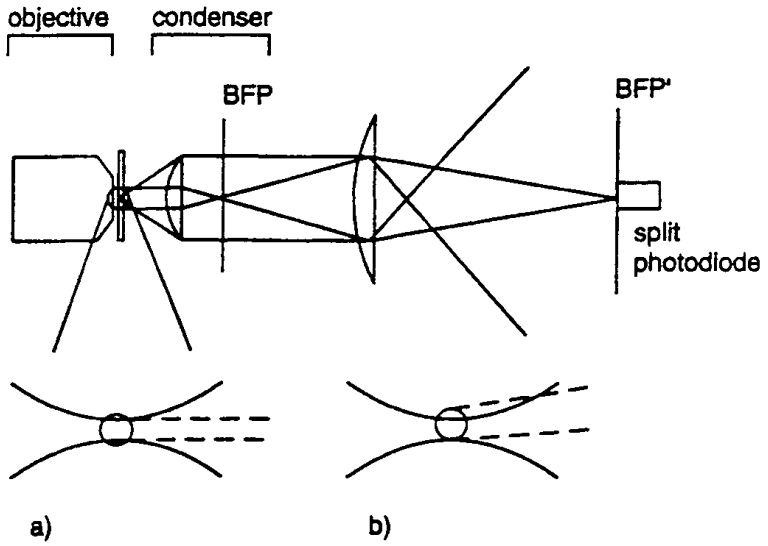

FIGURE 15.7 Working principle of forward-scattering detection method. When the particle is at the center of the optical trap, as shown in (*a*), the forward-scattered light is projected to the center of the split photodiode. When the particle is away from the center of the trap, as shown in (*b*), the forward-scattered light is projected off-center of the photodiode.

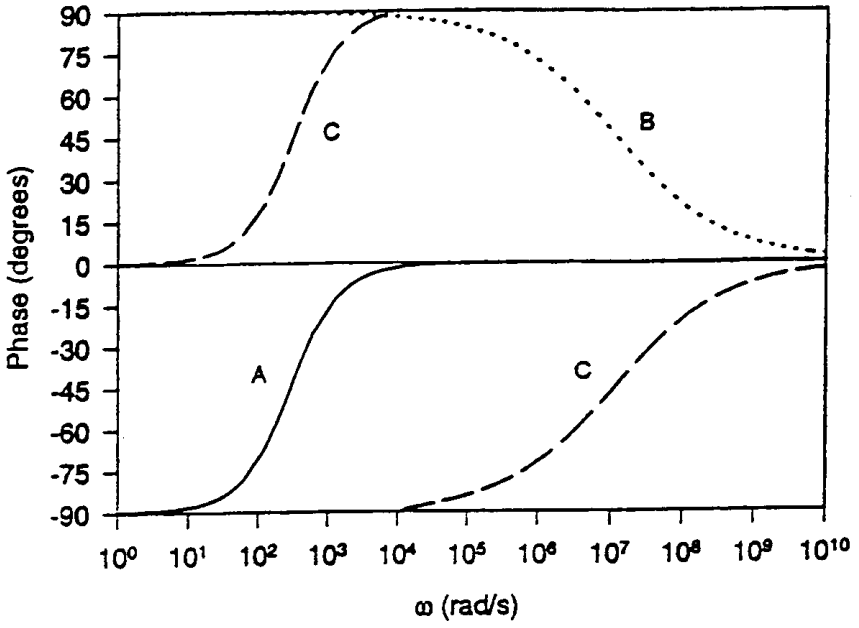

FIGURE 15.8 Plot of calculated phase shift in the moving trap reference frame δ vs. log (ω) for a 1.0-μm polystyrene particle (density 1.05 g/cm^3) in water (density = 1 g/cm^3, η_s = 0.01 poise). The spring constant k_{ot} is 3 mdyn/cm. The curve *A* is the moving frame phase shift δ′, the curve *B* is the first term, and curve *C* is the second term on the right side of Eq. (15.20).

The solution given in Eq. (15.16) is for the motion of a particle relative to the laboratory reference frame. Transformation between the two reference frames is straightforward. It can be shown that the measured phase shift in the trap frame is related to the phase shift in the laboratory frame by:

$$\delta'(\omega) = \tan^{-1}\frac{m^*\beta\omega}{m^*\omega^2 - k} + \tan^{-1}\frac{m^*\beta\omega}{(k + k_{ot}) - m^*\omega^2} \tag{15.18}$$

Note that the second term on the right side of the above equation is exactly the phase shift in the laboratory frame. Figure 15.8 shows each term in Eq. (15.18) as a function of log(ω). The curve *A* is the moving frame phase shift δ′, the curve *B* is the first term on the right side of the equation, and curve *C* is the second term.

The measured displacement in the trap frame, normalized to the amplitude of the trap motion, is

$$\frac{D'(\omega)}{A} = \sqrt{\frac{(m^*\beta\omega)^2 + (k - m^*\omega^2)^2}{(m^*\beta\omega)^2 + (k_{ot} + k - m^*\omega^2)^2}} \tag{15.19}$$

Figure 15.9 shows the relative displacement $D'(\omega)/A$, both as a function of log(ω).

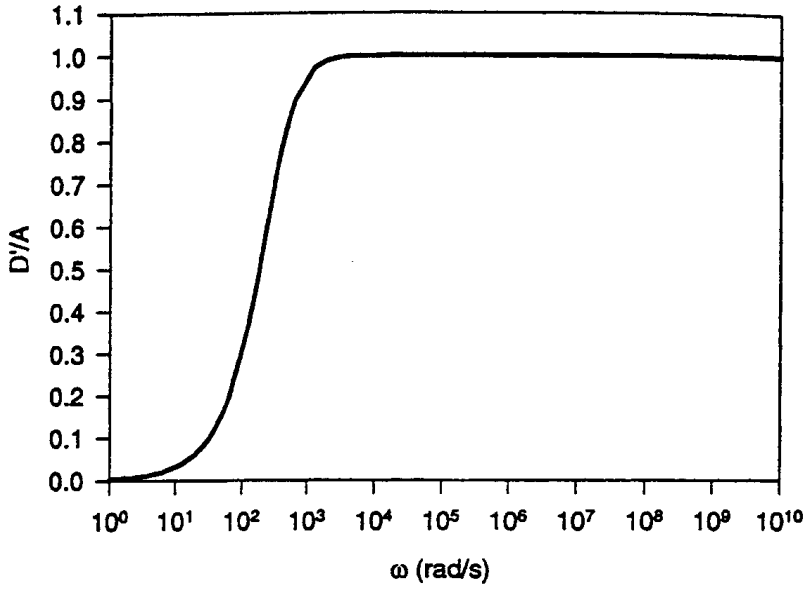

FIGURE 15.9 Plot of normalized displacement in the moving trap reference frame D'/A vs. log (ω) for a 1.0-μm polystyrene particle (density 1.05 g/cm^3) in water (density = 1 g/cm^3, η_s = 0.01 poise). The spring constant k_{ot} is 3 mdyn/cm.

In doing the forward-scattering measurements, we obtain directly the moving reference frame data for both phase shift δ' and displacement D'/A. To compare experimental phase shift δ' to Eq. (15.18) we can fit the equation to the data by iteration, where the spring constant k_{ot} is the only fitting parameter ($k = 0$ in water). The data were fit to the phase shift up to 90° (at 4000 rad/s), beyond which the data were not reliable. An error of a few degree near 90° phase shift can cause large errors in the fit. We believe the errors are caused by misalignment of the optical tweezers. Once the parameters are known, one can readily transform the data back to the laboratory reference frame. Figure 15.10 shows the laboratory frame phase shift δ versus log(ω) for a 1.1-μm diameter polystyrene latex sphere in water at the room temperature of about 23°C. (At the estimated laser power of less than 1 mW at the optical trap, we do not expect the trap temperature to be different from the ambient temperature.) The solid line is a fit to Eq. (15.18) with a laser power of 15 mW (reference power) measured just before the laser beam enters the microscope. Depending on the optical elements inside the microscope, only 2 to 5 % of the reference power reaches the focal point, where the optical tweezers are located; a precise percentage of the transmitted power is difficult to determine.

Figure 15.11 shows the trap frame displacement normalized to the amplitude of the trap motion. The condition of the experiments is the same as that shown in Figure 15.10. The displacement and phase shift data were taken simultaneously by the lock-in amplifier.

According to Eq. (15.11), the spring constant should be linearly proportional to the laser power at the optical trap. We carried out a calibration of the spring constant for 1.1-μm-diameter polystyrene particles and for similar sized

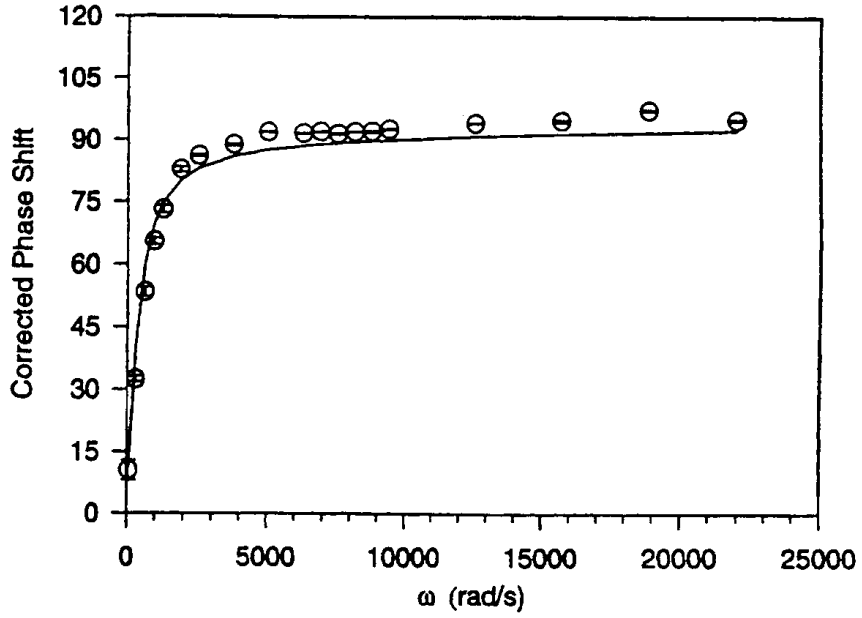

FIGURE 15.10 Laboratory frame phase shift δ vs. log (ω) for a 1.1-μm diameter polystyrene latex sphere in water at the room temperature of about 23°C.

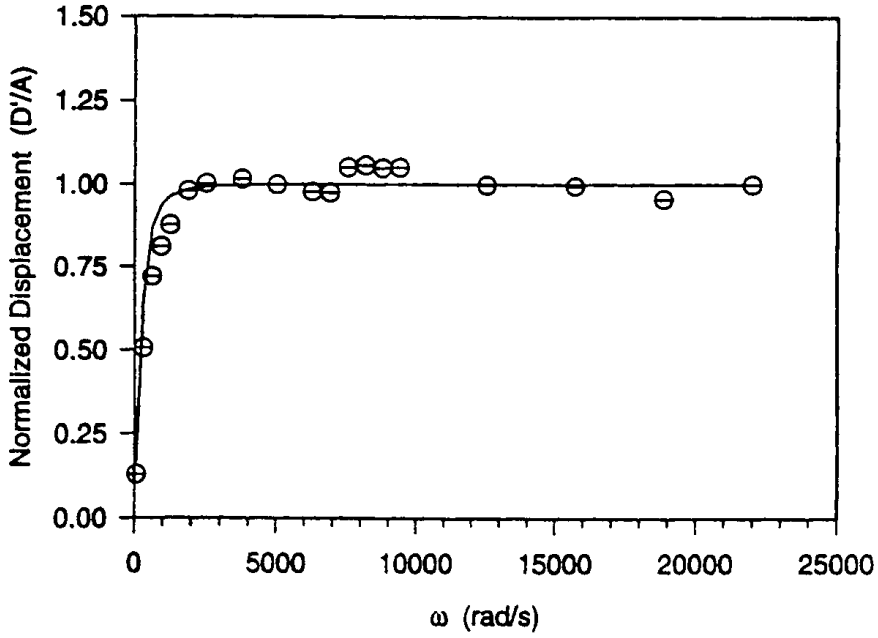

FIGURE 15.11 Trap frame displacement normalized to the amplitude of the trap motion. The condition of the experiments is the same as that shown in Figure 15.10. The displacement and phase shift data were taken simultaneously by the lock-in amplifier.

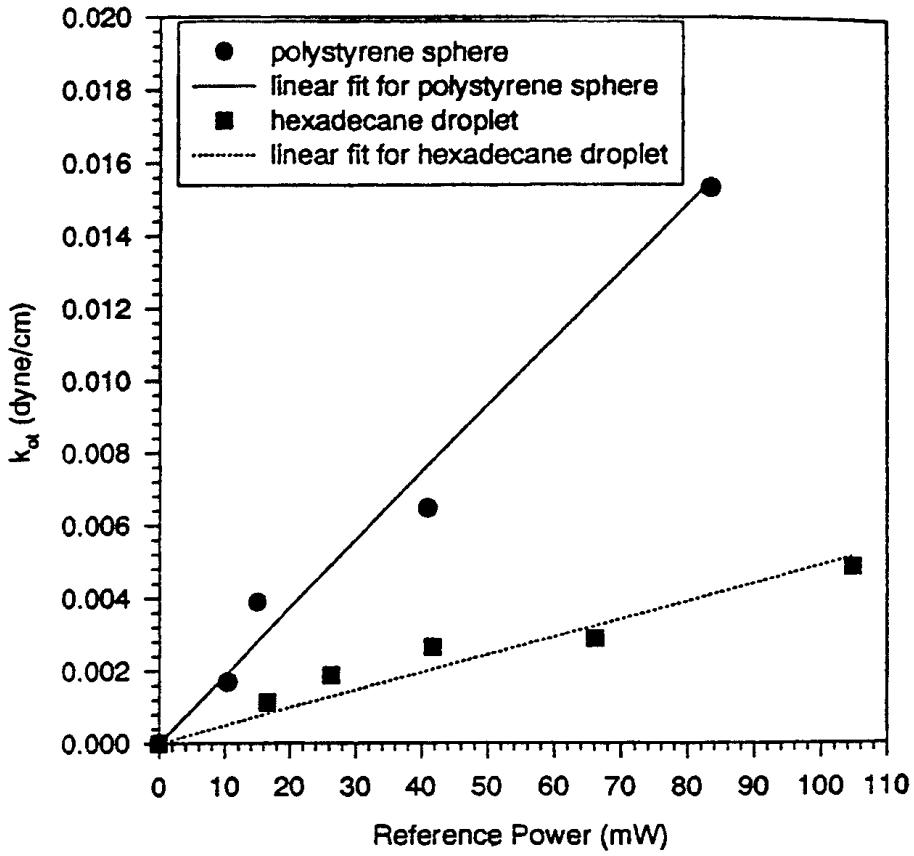

FIGURE 15.12 Plot of the measured spring constant vs. reference laser power. The linear relation between the spring constant and the laser power is predicted in Eq. 15.11.

surfactant-stabilized (TritonX-100) hexadecane oil droplets, both in pure water. As shown in Figure 15.12, reasonable linear fits are obtained for both the hard particles and oil droplets. The solid line in Figure 15.12 is not a best-fit line; instead it is calculated from Eq. (15.11) with all the known parameters for polystyrene particle, and with an assumption that $a = R$.

The dashed line in Figure 15.12 is a best fit to the oil droplet data. To calculate the spring constant for oil droplets in the trap is more difficult. The main difficulty is that the Stokes drag coefficient of the oil droplet may depend on the effects of surfactant molecules on the oil–water interface. The results shown here are based on the drag coefficient of a moving liquid particle in another liquid, with the assumption that the Marangoni effect is negligible. The drag coefficient is given by[16]

$$F_{\text{drag}} = -4\pi\eta a\left[\frac{1+(3\eta_{\text{oil}}/2\eta_s)}{1+(\eta_{\text{oil}}/\eta_s)}\right]V_\infty \tag{15.20}$$

where η_{oil} (= 3.032 cp) is the viscosity of the oil droplet and V_∞ is the fluid velocity far from the droplet.

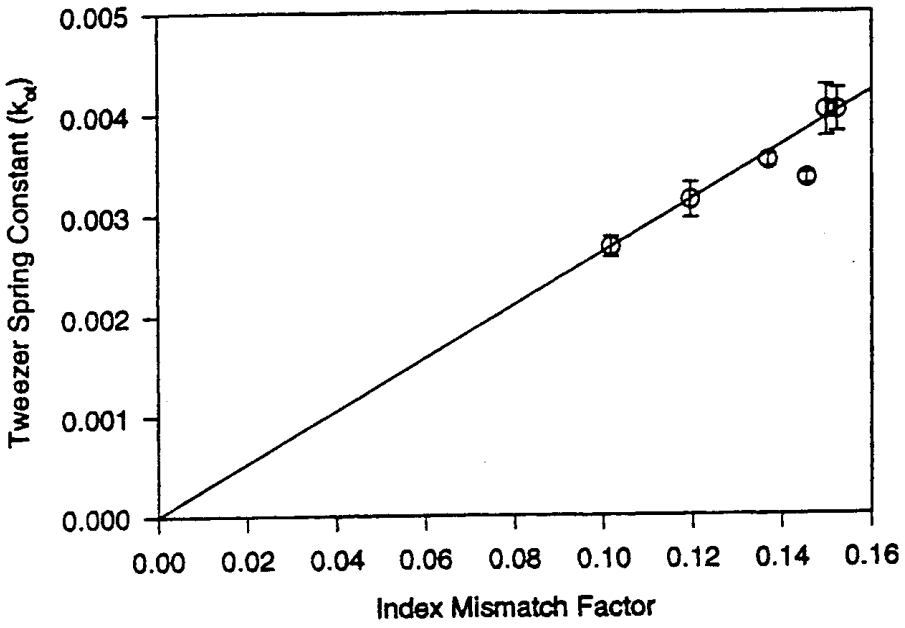

FIGURE 15.13 Measured spring constant vs. refractive index mismatch factor at a constant reference laser power of 15 mW. The data shown are for samples of weight percent of glycerol in water of 0, 5, 10, 20, 40 and 60. Because the refractive index of the glycerol (1.474) is higher than that of water, the highest glycerol content sample gives the lowest spring constant.

According to Eq. (15.11) the spring constant k_{ot} should be linearly proportional to the refractive index mismatch between the particle and the solution, that is,

$$k_{ot} \propto n_1 \frac{n_2^2 - n_1^2}{n_2^2 + 2n_1^2} \tag{15.21}$$

We carried out experiments in mixtures of water and glycerol to test this relationship. We chose water–glycerol mixtures because they cover a broad range of viscosity and a broad range in the refractive index mismatch. We took the viscosity of water–glycerol from the values given in the *CRC Handbook of Chemistry and Physics*[17] and calculated the refractive index mismatch by linear superposition of the refractive indices of water and glycerol according to the mass of each components. Figure 15.13 shows an excellent linear relationship between the measured spring constant k_{ot} and the calculated values of the refractive index mismatch, as is predicted in Eq. (15.21).

15.5.3. Forward-Scattering Method with Two Laser Beams

It is possible to measure the phase shift in the laboratory frame and still obtain broad frequency response by a forward-scattering method. This requires two laser

beams aligned colinearly at the optical trap. The first laser beam, linearly polarized, forms the stationary optical tweezers. The second laser beam, also linearly polarized but in a direction perpendicular to the first beam, forms the oscillating optical tweezers. Both optical tweezers act on the trapped particle and affect the motion of the particle. We let only the stationary laser beam reach the split photodiode detector by placing a polarizer between the optical tweezers and the detector to block the oscillating beam. The equation of motion for the particle is similar to that of Eq. (15.12), except that the effective spring constant k_{ot} on the left-hand side of the equation is replaced by the combined effective spring constant $(k_{ot1} + k_{ot2})$. With this approach, a reasonable response at high frequencies can still be achieved.

Figure 15.14 shows the data obtained by the two methods. In the dual-beam measurements the probe beam, forming the stationary optical trap, is more than an order of magnitude weaker in power than the oscillating beam. The oscillating beam here is at the same reference power as the single-beam experiments, thus we expect the spring constants measured by the two methods should be comparable. Indeed, as shown in Figure 15.14, the two sets of data gave a similar spring constant. Both sets of data in the figure are plotted (corrected) in the laboratory frame. The k_{ot} for the single-beam (trap frame) method is 4.130 mdyn/cm whereas the k_{ot} for the dual beam (laboratory frame) is 4.167 mdyn/cm. The major deviation of the data from best-fit lines that occurs at 60 Hz ($2\pi \cdot 60$ rad/s) is caused by the phase shift of the line frequency notch filter in the lock-in amplifier.

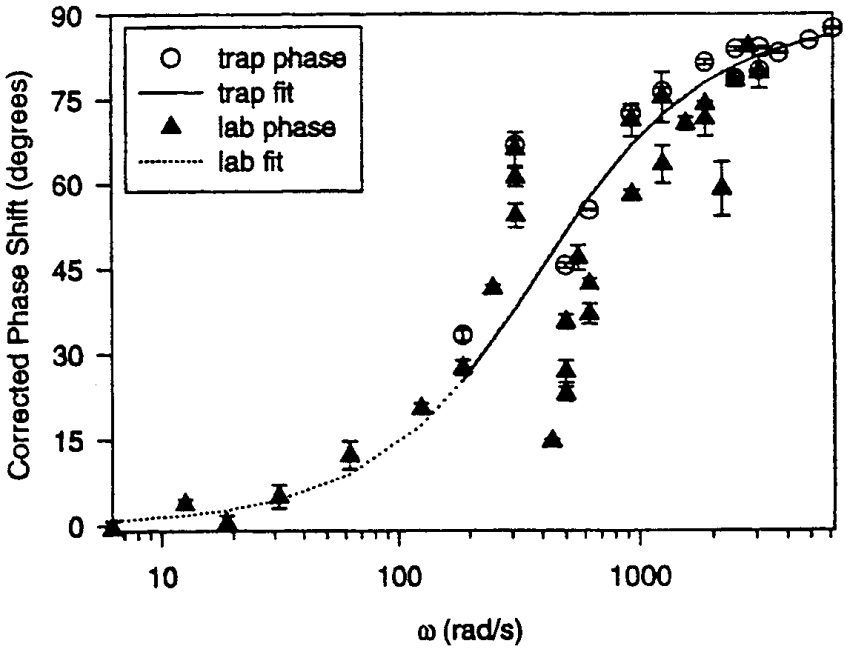

FIGURE 15.14 Comparison of the single laser beam and dual laser beam methods for measurement of the spring constant for a 1.1-μm polystyrene sphere in water at 23 °C and at 15 mW reference laser power

15.6. POTENTIAL APPLICATIONS

15.6.1. Microviscoelasticity

The equation of motion developed in Section 15.3 assumes constant solvent viscosity and elasticity. However, theory presented there can be readily extended so that the frequency-dependent microviscoelastic properties of polymer gels can be investigated. In this case, the solvent viscosity η_s and the medium elasticity k should be replaced by corresponding frequency-dependent functions. One can easily relate the frequency-dependent viscosity and elasticity to the storage and loss moduli $G'(\omega)$ and $G''(\omega)$. In general, one will need to measure both the phase and displacement response function to solve for $G'(\omega)$ and $G''(\omega)$.

Although the theory for macroscopic viscoelastic properties of associative polymer solutions is well established,[18,19] relatively little is known of the role of the adsorption of these polymers in the presence of the colloids to the rheological properties of the solution. In particular, the contrast between the case that polymers strongly adsorb and the cases that the polymers weakly adsorb or do not adsorb to the particles.[20] We suspect that the microviscoelasticity, the viscoelasticity measured within nanometer range of the particle surface, will be very different for each of the above cases. Thus, probing microviscoelasticity can provide valuable insight to the polymer–colloid interactions at the microscopic level, a key to a better understanding of the overall polymer–colloid solution rheology.[21]

15.6.2. Colloidal Forces Between Two Particles

The oscillating optical tweezers technique can also be used for probing dynamic interactions between two polymer-coated colloidal particles. In this case, the force on one of the particles is measured when a second particle, held by a separate optical tweezers, approaches.[22]

The most straightforward application might be probing hydrodynamic interactions between a pair of colloidal spheres. Theories for calculation of hydrodynamic interactions have been developed for decades,[23,24] however, few direct measurements of these interactions exist.[25] Hydrodynamic interactions occur when two particles move relative to each other. These motions are either from Brownian motion or from the forced oscillation discussed in this chapter. One ongoing experiment in our laboratory is to measure the Stokes drag of one oscillating particle as a second particle is approaching. The hydrodynamic force between particles moving in the longitudinal or shear directions is measured as a function of interparticle distance. Results of this study will be published elsewhere.

The applications to the two-particle interactions can be further extended for particles coated with polymers. Problems such as compression or shear forces between polymer brushes,[26–28] or bridging of polymers between two colloids[29,30] are just some possibilities of this kind of applications.

15.7. CONCLUSION

In this chapter, we demonstrate that it is possible to construct oscillating optical tweezers for dynamical measurements of forces on a single colloidal particle. The theoretical treatment includes the basic principle of optical tweezers and the solutions for the equations of motion of a particle driven into harmonic oscillation for both the laboratory reference frame and the optical trap reference frame.

A working experimental setup is provided to carry out tests using all three methods of detection: the imaging method, the single-beam forward-scattering method, and the dual-beam forward-scattering method. The imaging method gives reasonable results but suffers from limited frequency response. The single-beam forward-scattering method yields the best frequency response up to about 1 kHz, beyond which the results are found to be unreliable. We believe the errors at high frequencies are caused by misalignment of the optical tweezers. A phase error of a couple of degrees near the 90° phase shift can cause a large error in the data fitting. The dual-beam forward-scattering method compares well with the single-beam method and yields better data at low frequencies but cannot quite match the latter at the high frequencies.

Comparisons between experiments and theory are made for both solid polystyrene latex particles and for surfactant-stabilized hexadecane oil droplets. Water, dilute polymer in water solutions, and water–glycerol mixtures are used as solution media. Good agreements are made between the experiments and theory. Potential applications for microviscoelastic force measurements and possibilities to extend the applications of this technique to two-particle interactions are briefly mentioned.

Acknowledgments The author would like to acknowledge his graduate students, Luke E. Dewalt, Samantha J. Parmley, Joshua C. Daghlian, and Lawrence A. Hough and his two undergraduate students, Megan T. Valentine and Christopher J. Killian, all of whom performed the experiments. LED was supported by a Grant from the Polymer Interfaces Center, an NSF-IUCRC, at Lehigh University. SJP and JCD were supported by Graduate Fellowships from the U.S. Department of Education. LAH and CJK were supported by a grant from the National Science Foundation (SGER CTS-9805887). MTV was supported by a grant from NSF-REU Program at Lehigh University and a grant from the Lehigh University Forum Undergraduate Research.

REFERENCES

1. A. Ashkin, J. Dziedzic, J. Bjorkholm and S. Chu. *Opt. Lett.* **11**, 288 (1986).
2. S.M. Block. *Nature* **360,** 493 (1992). S.C. Kuo and M.P. Sheetz. *Trends Cell Biol.* **2**, 116 (1992). K. Svoboda and S.M. Block. *Annu. Rev. Biophys. Biomol. Struct.* **23**, 247 (1994). K. Svoboda, C.F. Schmidt, B.J. Schnapp and S.M. Block. *Nature* **365**, 721 (1993). K. Svoboda and S.M. Block. *Cell* **77**, (1994) 773.
3. J.C. Crocker and D.G. Grier. *Phys. Rev. Lett.* **73**, 352 (1994).

4. A. Ashkin. *Phys. Rev. Lett.* **24** 156 (1970). A. Ashkin and J.M. Dziedzic. *Science* **187**, 1073 (1975). J.P. Barton, D.R. Alexander and S.A. Schaub. *J. Appl. Phys.* **66**, 4594 (1989). W.H. Wright, G.J. Sonek and M.W. Berns. *Appl. Phys. Lett.* **63**, 715 (1993).
5. L.P. Ghislain, N.A. Switz and W.W. Webb. *Rev. Sci. Inst.* **65**, 2762 (1994).
6. R.M. Simmons, J.T. Finer, S. Chu and J.A. Spudich. *Biophys. J.*. **70**, 1813 (1996).
7. A. Ashkin, J.M. Dziedzic, J.E. Bjorkholm and S. Chu. *Opt. Lett.* **11**, 288 (1986).
8. S.C. Kuo, *J. Microscopy Soc. Am.* **1**, 65 (1995).
9. M.T. Valentine, L.E. Dewalt and H.D. Ou-Yang. *J. Phys: Condens. Matt.* **8**, 9477 (1996).
10. M.T. Valentine and H.D. Ou-Yang. 71st Colloid and Surface Science Symposium Abstracts, No. 143 (1997).
11. A. Ashkin, *Science* **210** (4474), 1081 (1980).
12. A. Ashkin. *J. Biophys.* **61**, 569 (1992).
13. J.D. Jackson, *Classical Electrodynamics* 2nd ed, Sect 4.7, Wiley, New York, 1975.
14. L.D. Landau and E.M. Lifshitz. *Fluid Mechanics* Pergaman, Oxford, 1982.
16. A.Y. Rednikov, Y.S. Ryazantsev and M.G. Velarde. *Phys. Fluids* **6**, 451 (1994).
17. D.R. Lide, *CRC Handbook of Chemistry and Physics*, 73rd ed., CRC Press, Boca Raton, FL, 1992–93.
18. F. Tanaka and S.F. Edwards. *J. Non-Newtonian Fluid Mech.* **43** 247 (1992).
19. R.D. Jenkins. Ph.D Thesis, Lehigh University, 1991.
20. Y.W. Inn and S.Q. Wang. *Phys. Rev. Lett.* **76** 467 (1996).
21. M.T. Valentine, L.E. Dewalt and H.D. Ou-Yang. *Res. Prog. Rep.* **12**, 68 (1997).
22. H.D. Ou-Yang. 71st Colloid and Surface Science Symposium Abstracts, No. 268 (1997).
23. G.K. Batchelor. *J. Fluid Mech.* **74**(1), 1 (1976).
24. S. Kim and S.J. Karrila. *Microhydrodynamics: Principles and Selected Applications* Butterworth-Heinemann, Boston, 1991.
25. J.C. Crocker. *J. Chem. Phys.* **106**, 2837 (1997).
26. J. Klein, D. Perahia and S. Warburg. *Nature* **352**, 143 (1991).
27. G.S. Grest. *Phys. Rev. Lett.* **76**, 4979 (1996).
28. P.S. Doyle, E.S.G. Shaqfeh and A.P. Gast. *Phys. Rev. Lett.* **78**, 1182 (1997).
29. L.E. Dewalt, Z Gao and H.D. Ou-Yang. *ACS Adv. Chem.*, **248**, 395 (1996).
30. A. Johner and J.F. Joanny, *J. Chem. Phys.* **98**, 1647 (1993).